*International Tables for X-ray Crystallography* (1952), vol. 1. Birmingham: Kynoch Press.
MACGILLAVRY, C. H. & BRUINS, E. M. (1948). *Acta Cryst.* **1**, 156.
PAULING, L., COREY, R. B., YAKEL, H. L. JR. & MARSH, R. E. (1955). *Acta Cryst.* **8**, 853.
STOKES, A. R. (1955). *Acta Cryst.* **8**, 27.
STRATTON, J. A. (1941). *Electromagnetic Theory*, chap. 6. New York: McGraw-Hill.
TITCHMARSH, E. C. (1937). *Theory of the Fourier Integral.* Oxford: Clarendon Press.
WASER, J. (1955). *Acta Cryst.* **8**, 142.
WATSON, J. D. (1954). *Biochim. Biophys. Acta*, **13**, 10.
WATSON, J. D. (1957). *The Chemical Basis of Heredity.* Baltimore: Johns Hopkins Press.
WATSON, J. D. & CRICK, F. H. C. (1953). *Nature, Lond.* **171**, 737.
WHITTAKER, E. J. W. (1955). *Acta Cryst.* **8**, 571.
WILKINS, M. H. F., STOKES, A. R. & WILSON, H. R. (1953). *Nature, Lond.* **171**, 737.
WYCKOFF, H. W. (1955). Thesis, Massachusetts Institute of Technology.

*Acta Cryst.* (1958). **11**, 213

# Tobacco Mosaic Virus: Application of the Method of Isomorphous Replacement to the Determination of the Helical Parameters and Radial Density Distribution

BY ROSALIND E. FRANKLIN AND K. C. HOLMES

*Birkbeck College Crystallography Laboratory (University of London), 21 Torrington Square, London W. C. 1, England*

(*Received* 8 *August* 1957)

It is known that in tobacco mosaic virus (TMV) structurally equivalent protein sub-units lie in helical array about the long axis of the rod-shaped particle. It has not, however, proved possible to make a reliable determination of the helical parameters by the usual methods of direct measurement on X-ray fibre diagrams.

A quantitative comparison has now been made of the equatorial intensities in fibre diagrams of TMV and of a mercury-substituted TMV, TMV-Hg. This has led to the determination, first of the radial distance of the substituted mercury from the particle axis in TMV-Hg, and then of the parameters of the helical arrangement of protein sub-units in TMV. It also made possible the calculation of the radial density distribution in TMV, the result obtained being in good agreement with the earlier work of Caspar.

From a knowledge of the helical parameters and other physical and chemical data it can be shown that the symmetry of TMV is that of the simplest possible helical line group, there being no symmetry elements other than the helical axis.

## Introduction

The X-ray fibre-diagrams obtained from orientated preparations of tobacco mosaic virus (TMV) show that the particles have a highly ordered internal structure (Bernal & Fankuchen, 1941). The best fibre diagrams are obtained from concentrated aqueous gel preparations in thin-walled glass capillary tubes (Bernal & Fankuchen, 1941), in which the virus particles, of length about 3000 Å (see Williams & Steere, 1951) and mean diameter about 150 Å (Bernal & Fankuchen, 1941; Franklin & Klug, 1956) lie with their long axes parallel to the axis of the tube. Since the virus particles are in random rotation about their long axes, and, moreover, do not lie strictly on a lattice, these fibre diagrams record, effectively, the cylindrically averaged squared structure factor of a *single* virus particle; interparticle interference effects are appreciable only on the equator at spacings larger than 100 Å.

Certain features of the structure of the virus can be deduced directly from measurements made on TMV fibre diagrams alone. In this way it has been shown (Watson, 1954; Franklin, 1955) that the virus protein (which comprises about 94% of the virus, the remainder being ribonucleic acid (RNA)) consists of equivalent sub-units set in helical array about the particle axis, the axial repeat period of 69 Å containing $3n+1$ such sub-units on 3 turns of the helix. It was also shown (Franklin & Klug, 1956) from a direct study of TMV fibre diagrams that the surface of the TMV particle is not smooth, but bears a rather deep helical groove, between the turns of which lies a helical array of knobs.

While it is possible to push somewhat further this type of direct interpretation of the TMV diagrams, more substantial progress can be made by comparing these diagrams with those of related substances. It has been shown by Green, Ingram & Perutz (1954)

that the method of isomorphous replacement can be usefully employed in problems of protein structure. This paper describes the first steps towards a systematic application of this method to the study of the structure of TMV.

## Helical parameters

In discussing the helical parameters of TMV we shall use the terminology of Klug, Crick & Wyckoff (1958, hereafter referred to as K.C.W.). It will be convenient to describe the helical structure of TMV protein in terms of its *basic* helix (see K.C.W.), this being fully defined by $u$, the number of structure units in the axial repeat period, $t$, the number of turns of the helix per repeat, and $P$, the pitch of the helix. Here the structure unit may be considered as the analogue of the unit cell of a crystal; the helical parameters are analogous to the unit-cell dimensions. Like the unit cell of a crystal, the structure unit can contain more than one asymmetric unit. That is, in the terminology of K.C.W., the structure may contain more than one asymmetric chain.

When the helical structure is viewed in the form of its radial projection (see K.C.W.), there is one helical net point for each structure unit. The parameter $u$ thus also defines the number of helical net points per repeat.

Pursuing further the analogy with a crystal, we find that it is, in theory, possible to determine the helical parameters from direct measurements on the appropriate X-ray diagrams. (Moreover, for this, the fibre diagram is not only the one which is most often available, but is also that which is ideally suited to the purpose.) It is necessary only to establish the order, $n$, of the Bessel function terms which contribute to a number of different layer-lines, $l$, and then to apply the selection rule (see K.C.W.)

$$n = (mu+l)/t\,, \qquad (1)$$

where $n$ and $m$ are integers.

However, although this method has been successfully applied to a number of simpler structures (Bunn & Howells, 1954; Wilkins, Stokes & Wilson, 1953; Franklin & Gosling, 1953; see also Crick, 1954), attempts to apply it to TMV have led to two erroneous estimates of $u$. We shall therefore first explain how these mistakes arose, and then proceed to describe a method which we believe gives the value of $u$ much more reliably.

It is immediately obvious, from inspection of the TMV fibre diagram, that Bessel functions of low order occur on layer lines 3, 6, and 9. Moreover the positions of the innermost intensity maxima on the 3rd layer line (taken in conjunction with the known maximum radius of the virus particle, 80–90 Å (Franklin, 1955; Franklin & Klug, 1956), are such that they could be due only to a Bessel function of the first order (see Franklin & Klug, 1956). The positions of the innermost maxima on the 6th and 9th layer lines are consistent with their being due to $J_2$ and $J_3$ terms respectively.

The occurrence of $J_1$, $J_2$ and $J_3$ terms on layer lines 3, 6, and 9 respectively gives two pieces of information concerning the helical structure. First, it follows from the selection rule (1), that $t = 3$. That is, the 3rd layer line is that which relates to the pitch of the helix, 23 Å. Secondly, the structure must belong to one of the helical line groups which does *not* have rotational symmetry, since the presence of $r$-fold rotational symmetry would lead to the absence of all $J_n$ for which $n$ is not a multiple of $r$. Thus, in the notation of K.C.W., the structure belongs *either* to the simplest helical line group, $s$, *or* to the group $s2$, which has dyads perpendicular to the helical axis. Hence, in TMV, there must be either one or two asymmetric units (K.C.W., Table 1) per helical net point.

It remains to determine the value of $u$. It follows from the selection rule, (1), that a zero-order Bessel function occurs on the $u$th layer line. Since $J_0$ is the only Bessel function which has a maximum at the origin, the value of $u$ may be determined by finding which is the first layer line (after the equator) which bears a truly axial intensity maximum. The spacing of this axial intensity maximum will correspond to the axial distance between successive helical net points.

By taking photographs of tilted specimens, Watson (1954) observed a strong, apparently axial maximum on the 31st layer line, and suggested that $u$ might be 31. In photographs of better orientated preparations Franklin (1955) showed that the maximum on the 31st layer line was not truly axial (Fig. 1). She observed a further maximum on the 37th layer line, which was not split, and therefore suggested the value 37 for $u$. This method of determining $u$ for TMV is, however, highly unreliable, since the maximum radius of the helix is so large that the slightest lack of orientation in the specimen makes it impossible to distinguish between a Bessel function of zero and one of low but non-zero order. This is true even if the angle of tilt of the specimen is accurately known. For example, taking the maximum radius of the particle to be 80 Å, the position of the maxima on the 31st layer line, shown in Fig. 1, is such that they could be due to a Bessel function of order as high as 14. It is thus clearly hopeless to attempt to distinguish, by this method, between Bessel functions of order 0, 1, 2 or 3. We therefore made a fresh approach to the problem, using the method of isomorphous replacement.

## Isomorphous replacement

The method of isomorphous replacement is normally employed for the determination of the signs and phases of structure factors of a crystal after the unit cell and space group have been determined. In the case of TMV, however, it has proved useful to introduce it at an earlier stage of the investigation. If each structure

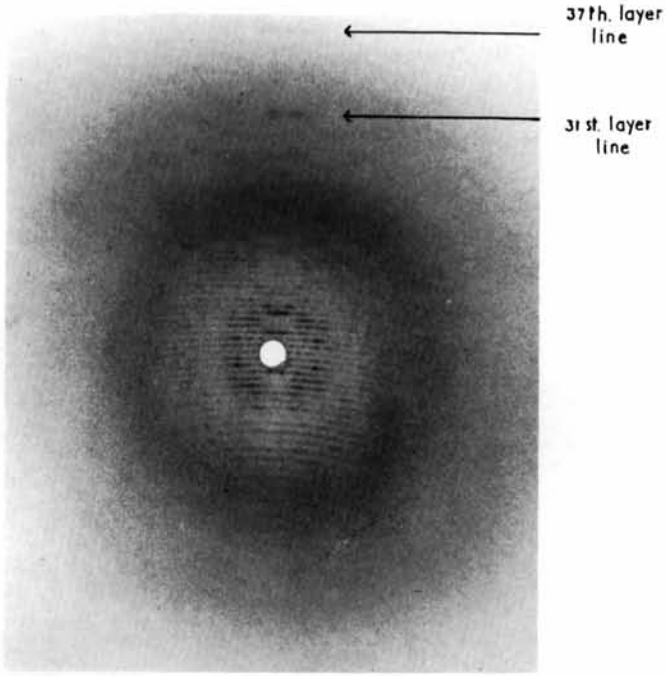


Fig. 1. X-ray fibre diagram of orientated TMV solution, showing splitting of the intensity maximum on the 31st layer line. The axis of the specimen was inclined at about 20° to the vertical, this being the angle required for a *complete* representation of the 31st layer line.

For this photograph an Ehrenberg–Spear fine-focus X-ray tybe was used, with a hydrogen-filled camera and lead-glass capillary collimator of bore 50$\mu$. Specimen–film distance 11 mm., exposure time 137 hr.

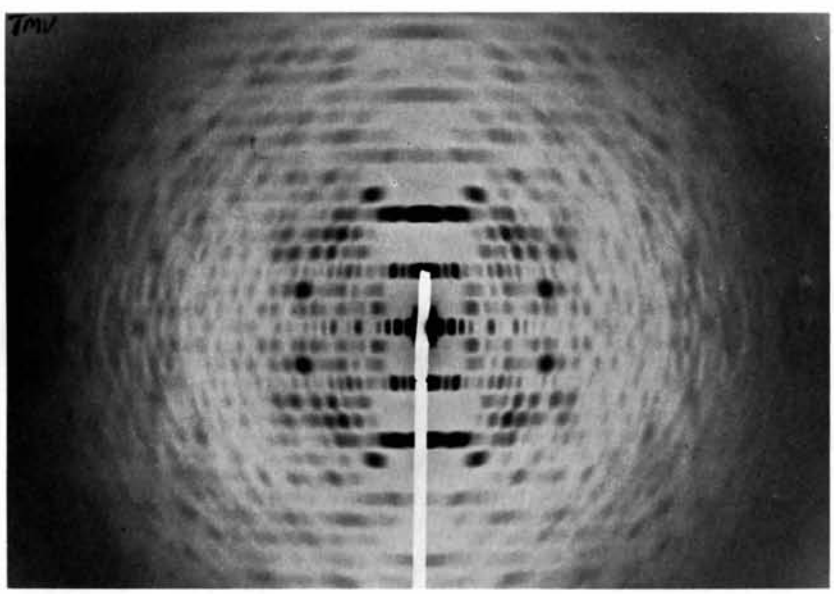

Fig. 2. X-ray fibre diagram of orientated TMV solution, with axis of specimen vertical. For this photograph a bent-quartz line-focusing monochromator was used, with a vacuum camera having a specimen–film distance of 12 cm.

[*To face p.* 214

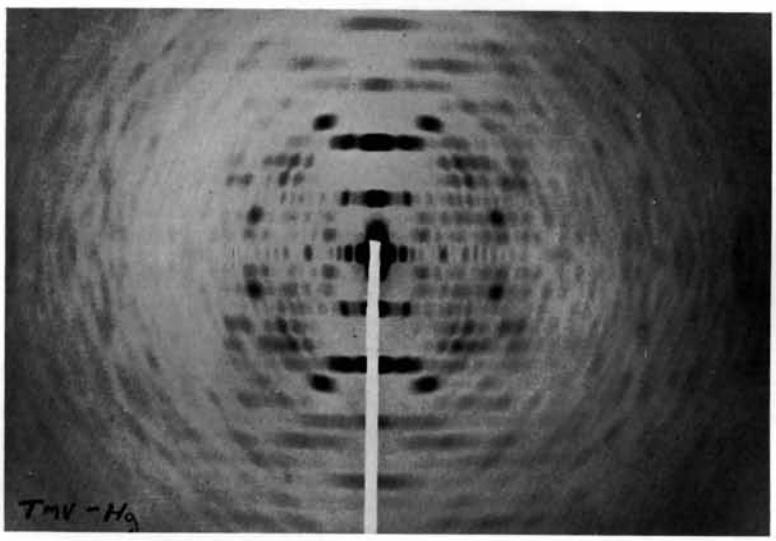


Fig. 3. X-ray fibre diagram of orientated solution of the mercury derivative of TMV, TMV-Hg. Camera etc. the same as for Fig. 2.

unit can be labelled in a specific way with a heavy atom, it is possible, from a detailed comparison of the X-ray fibre diagrams of TMV and its heavy-atom derivative, to measure, in effect, the X-ray fibre diagram of the helical array of heavy atoms, and hence to determine the helical parameters.

The selection rule, (1), shows that, in addition to a $J_0$ contribution on layer lines $u$, $2u$, etc., there are contributions of $J_0$, $J_u$, $J_{2u}$, etc., on the equator. This paper describes the use of a heavy-atom derivative of TMV to detect the equatorial $J_u$ contribution and determine its order, $u$. The work falls into two parts. First, in the low-angle region of the equator, where scattering is due to $J_0$ contributions only, a quantitative comparison of scattering by TMV and a mercury derivative of TMV (TMV-Hg) enabled the radial distance of the mercury from the helical axis to be determined. Then, from a comparison of the scattering of the two materials at higher angles, it was possible to identify the first peak of the $J_u$ contribution due to the mercury atoms, and hence, knowing the radius at which the mercury lies, to find the value of $u$.

The first stage of the work leads also to the determination of the *signs* of the particle scattering factor in the angular range in which only $J_0$ terms are important. These were used to calculate the radial density distribution in the virus. The radial density distribution so obtained is in good general agreement with that derived by Caspar (1955; 1956) using a different heavy-atom derivative.

## The heavy-atom derivative

Measurements were made on a normal strain of TMV and on its mercury derivative, TMV-Hg. Both these substances were prepared for us by Dr H. Fraenkel-Conrat at Berkeley. In TMV-Hg, mercury in the form of $-Hg-CH_3$, was bound to the extent of one atom to approximately 20,000 molecular weight of virus. Chemical investigations have shown that TMV protein is built up of sub-units of molecular weight 17,000–18,000 (Harris & Knight, 1952, 1955; Schramm & Braunitzer, 1953; Braunitzer, 1954; Schramm, Braunitzer & Schneider, 1954). The TMV-Hg preparation therefore contains nearly one mercury atom to each sub-unit. Moreover, the mercury is bound to the cystein, and there is only one cystein residue in each chemical sub-unit (Knight, 1954). If we make the reasonable assumption that all chemical sub-units are structurally equivalent as far as the X-ray fibre-diagrams are concerned (which does not necessarily imply that they are all chemically identical in every detail), it follows that the chemical sub-unit is the 'asymmetric unit' of the helical structure. There are thus either 1 or 2 Hg sites (that is, either 1 or 2 chemical sub-units) to each helical net point, according to whether the line group of the helical structure is $s$ or $s2$ (see above). Moreover, the mercury atoms must all lie in structurally equivalent positions; that is, they must all lie at the same distance from the helical axis in a helical arrangement whose parameters, $u$ and $t$, are the same as those of the helix of the virus protein.

## Experimental

Both the TMV and TMV-Hg preparations were used in the form of concentrated aqueous solution (about 20–30% virus) sealed in thin-walled glass capillary tubes of diameter about 0·5 mm.

X-ray fibre diagrams were obtained with Cu $K\alpha$ radiation, using a bent-quartz line-focusing monochromator. The specimen–film distance was 12 cm., and the camera was continuously evacuated.

Intensities were measured with the Walker recording microdensitometer (Walker, 1955). Multiple-film exposures were used, and measurements were confined to regions of photographic density less than 0·8. In addition, photographs with somewhat weaker exposures were taken with one half of the film shielded by an aluminium screen which transmitted 0·26 of the incident Cu $K\alpha$ radiation. This was necessary in order to relate the intensity of the first (non-origin) equatorial peak to measurements on the rest of the photograph, since the intensity of this peak was about ten times as great as that of the next strongest peak.

## The analysis

X-ray fibre diagrams of TMV and TMV-Hg, obtained with the focusing camera, are shown in Figs. 2 and 3. In this paper we shall be concerned only with the detailed analysis of the equatorial regions.

The structure factor on the equator is given by:

$$F = \text{Const.} \times [\sum_j f_j J_0(2\pi R r_j) + 2 \sum_j f_j J_u(2\pi R r_j) \times \exp[iu(\psi - \varphi_j + \tfrac{1}{2}\pi)] + 2 \sum_j f_j J_{2u}(2\pi R r_j) \exp[2iu(\psi - \varphi_j + \tfrac{1}{2}\pi)] + \text{etc.}], \quad (2)$$

where $f_j$ is the scattering factor of the atom $j$ which has coordinates $r_j$, $\varphi_j$, and $R$ and $\psi$ are the corresponding reciprocal-space coordinates. We know, from earlier work (Watson, 1954; Franklin, 1955), that $u$ cannot be less than 37 and that the radius of the particle is not greater than 80–90 Å. It follows that terms in $J_{2u}$ and higher orders occur only at very large angles and are outside the range of our measurements. We are therefore concerned only with terms in $J_0$ and $J_u$.

### *The $J_0$ term*

If the radius of the particle is 80 Å and $u$ not less than 37, the value of the $J_u$ term cannot differ significantly from zero for values of $R (= 2 \sin\theta/\lambda)$ less than 0·08 Å$^{-1}$. In practice, we have been able to distinguish between the $J_0$ and $J_u$ contributions, and hence to measure the $J_0$ term, for values of $R$ up to 0·10 Å$^{-1}$. This is possible because, in the range $R =$ 0·06–0·10 Å$^{-1}$, there is a rather regular alternation of

intensity of period so small that it corresponds to a structure of radius 73 Å, which is close to the maximum radius of the virus particle. This part of the intensity pattern must therefore be due to the $J_0$ term, since the first few peaks of a high-order Bessel function are much broader than succeeding ones, and so could not possibly produce such an effect. Moreover, since the structure factor of the $J_0$ term is everywhere real, we know that the $J_0$ term must pass through zero between each of these closely spaced intensity maxima (cf. Bragg & Perutz, 1952). These considerations make it possible to insert semi-empirically, on the microdensitometer traces, the smooth curve of the background scattering which must be subtracted from the total scattering in order to obtain the $J_0$ term. The background so subtracted is due mainly to scattering by glass and water, but could also contain a small contribution from the $J_u$ term.

From the $J_0$ part of the intensity curves, derived in this way, $F$ ($= \sqrt{I}$) was calculated for both TMV and TMV-Hg.

Assuming (for the reasons given above) that all the mercury atoms in TMV-Hg lie at the same radius, $r_{\mathrm{Hg}}$, then the difference between the $J_0$ terms of $F_{\mathrm{TMV}}$ and $F_{\mathrm{TMV\text{-}Hg}}$ will be a simple Bessel function of the form $AJ_0(2\pi Rr_{\mathrm{Hg}})$, where $A$ is an amplitude related to the mercury concentration. $F_{\mathrm{TMV}}$ and $F_{\mathrm{TMV\text{-}Hg}}$ (and hence $I_{\mathrm{TMV}}$ and $I_{\mathrm{TMV\text{-}Hg}}$) must therefore be equal at values of $R$ corresponding to the nodes of $J_0(2\pi Rr_{\mathrm{Hg}})$.

On the basis of the above considerations, a good preliminary estimate of $r_{\mathrm{Hg}}$ can be obtained by direct inspection of the equatorial intensity curves for TMV and TMV-Hg, using only a few of the most obvious points of difference between the two curves. Particularly valuable for this purpose is the observation that several of the equatorial intensity maxima of TMV are *displaced* in TMV-Hg and yet not appreciably broadened. This means that the mercury contribution changes sign somewhere within these TMV intensity peaks, thus obliterating one edge of the peak and extending the other. This effect is most marked for the peak at $R = 0{\cdot}052$ Å$^{-1}$, which is displaced outwards in TMV-Hg. In addition, the peaks at $R = 0{\cdot}069$ Å$^{-1}$ and $R = 0{\cdot}077$ Å$^{-1}$ are displaced inwards (see Fig. 4).

The approximate position of three of the nodes of $J_0(2\pi Rr_{\mathrm{Hg}})$ can then be located in this way. Further, the peaks at $R = 0{\cdot}028$ Å$^{-1}$ and $R = 0{\cdot}036$ Å$^{-1}$ are both strongly reduced in intensity in TMV-Hg, without any significant shift in the *positions* of maximum intensity. These two peaks are so sharp and so close together that they must be of opposite sign, so it follows that the mercury contribution must change sign between the two peaks. Another node of $J_0(2\pi Rr_{\mathrm{Hg}})$ must therefore be located close to $R = 0{\cdot}032$ Å$^{-1}$.

From these observations alone it was concluded that the value of $r_{\mathrm{Hg}}$ was close to 57 Å. This is illustrated in Fig. 5, where the function $J_0(2\pi Rr_{\mathrm{Hg}})$ is shown for

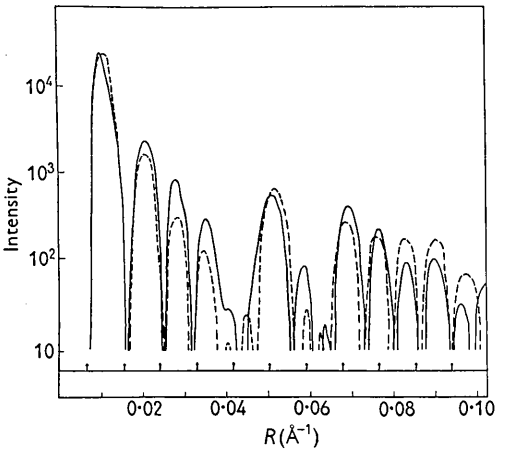


Fig. 4. The intensity distribution on the equator for TMV (full-line curve) and TMV-Hg (broken curve) plotted, on a logarithmic scale, as a function of $R$. The arrows on the base line indicate the positions of the nodes of $J_0(2\pi R \times 56{\cdot}2)$. If the mercury atoms in TMV-Hg lie at a radial distance of 56·2 Å from the particle axis, $I_{\mathrm{TMV}}$ and $I_{\mathrm{TMV\text{-}Hg}}$ should be equal at these positions, if the mercury substitution is strictly isomorphous.

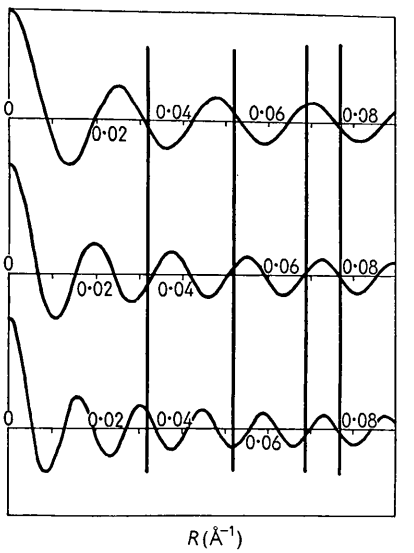


Fig. 5. Plot of the functions $J_0(2\pi R \times 44{\cdot}5)$ (top), $J_0(2\pi R \times 57)$ (middle), and $J_0(2\pi R \times 70)$ (bottom). The heavy vertical lines indicate approximate positions of nodes of $2\pi Rr_{\mathrm{Hg}}$, deduced from inspection of the equatorial intensity curves for TMV and TMV-Hg. The function $J_0(2\pi R \times 57)$ gives the best fit with these positions.

$r = 57$ Å and also for two values of $r$ (44·5 Å and 70 Å) which give the next-best fits with the positions of the nodes deduced above. The only satisfactory fit with all four of these nodal positions is obtained for values of $r$ close to 57 Å.

To obtain $r_{\mathrm{Hg}}$ with greater precision it is necessary first to determine the relative scale of our two sets of

intensity measurements (for TMV and TMV-Hg) and then to determine the experimental difference curve, $F_{\text{TMV-Hg}}-F_{\text{TMV}}$.

To determine the relative scale of the two intensity curves, logarithmic plots of $I_{\text{TMV}}$ and $I_{\text{TMV-Hg}}$ were prepared, superimposed on one another (see Fig. 4), and translated with respect to one another in the direction of the $I$ axis until a position was found in which the two curves intersected at all the nodes of a function $J_0(2\pi Rr_{\text{Hg}})$, for a possible value of $r_{\text{Hg}}$. (There are, of course, other intersections, where $F_{\text{TMV}}$ and $F_{\text{TMV-Hg}}$ are of equal magnitude but opposite sign.) It was found that there was only one way in which this could be done, and this gave a value of $r_{\text{Hg}} = 56{\cdot}2 \pm 1{\cdot}0$ Å, in satisfactory agreement with the above preliminary estimate of 57 Å for $r_{\text{Hg}}$.

In Fig. 4 the positions of the nodes of $J_0(2\pi R \times 56{\cdot}2)$ are shown, together with the two intensity curves. (At the suggestion of Dr F. H. C. Crick, the relative intensity scale was also determined from the relationship

$$\frac{\Sigma R|F_{\text{TVM}}|}{\Sigma R|F_{\text{TVM-Hg}}|} = \left(\frac{F_{\text{TMV}}}{F_{\text{TMV}}+F_{\text{Hg}}}\right)_{R=0}.$$

The scaling factor obtained in this way agreed to within 1·5% with that obtained by the method described above.)

It will be noted that the operation described above results in the simultaneous determination of both the radius at which the mercury atoms lie, and the *signs* of the $J_0$ part of the TMV structure factor, since the signs of the mercury contribution are everywhere fixed once $r_{\text{Hg}}$ is known. The signs determined in this way agree with those obtained earlier by Caspar (1955, 1956) from a comparison of scattering by TMV and by a lead derivative of the virus. Using these signs, the $J_0$ terms of the structure factor of TMV and TMV-Hg are shown in Fig. 6.

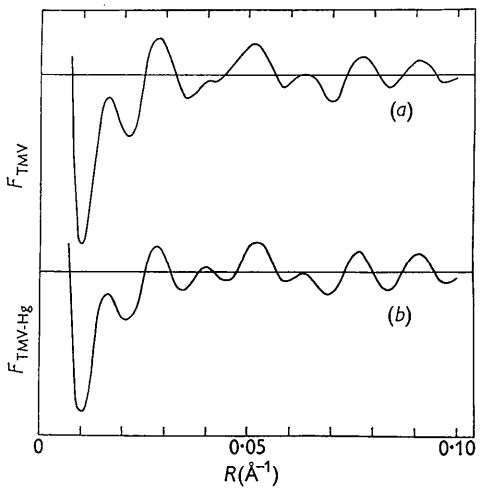


Fig. 6. The $J_0$ terms of the structure factors of (*a*) TMV and (*b*) TMV-Hg on the equator of the X-ray fibre diagrams, for values of $R$ between 0·0076 and 0·10 Å$^{-1}$.

In Fig. 7 the experimental difference between $F_{\text{TMV}}$ and $F_{\text{TMV-Hg}}$ is compared with the function

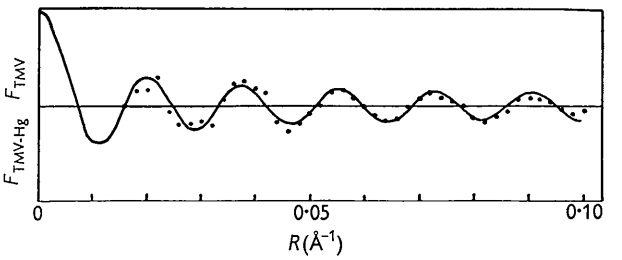


Fig. 7. The difference between the measured values of $F_{\text{TMV-Hg}}$ and $F_{\text{TMV}}$ (dotted line) is compared with the function $AJ_0(2\pi R \times 56{\cdot}2)$ (full line). The value of $A$ for the theoretical function here shown is such that, at $R = 0$, $F_{\text{Hg}}$ is approximately 5% of $F_{\text{TMV}}$ (see text).

$J_0(2\pi R \times 56{\cdot}2)$. In the range $R = 0{\cdot}02$–$0{\cdot}10$ Å$^{-1}$ agreement between the observed and theoretical difference curves is satisfactory. At lower values of $R$ there is some distortion of the experimental values due to inter-particle interference, while at the highest values of $R$ measurements are less accurate because of the increasing importance of the semi-empirical background correction (see above).

*The $J_u$ term*

Since the first peak of a high-order Bessel function is broad, the term $2J_u(2\pi Rr_{\text{Hg}})$ will be identifiable by a broad maximum or minimum in intensity present on the equator of TMV-Hg and absent in TMV. Such a maximum is clearly visible in the region of $R = 0{\cdot}14$ Å$^{-1}$. Since no similar effect is observed at smaller values of $R$, this must be the first peak of $2J_u(2\pi Rr_{\text{Hg}})$.*

Earlier work, involving measurements of the first peak on each layer line, led to the conclusion that $u$ is $3n+1$ rather than $3n+2$ ($u$ could not be $3n$, since this would mean that layer lines 1, 2, 4, 5, etc. would vanish). Figs. 8(*a*) and 8(*b*) show equatorial photometer traces for TMV and TMV-Hg in the region of the first peak of $2J_u(2\pi Rr_{\text{Hg}})$, and in Fig. 8(*c*) the measured values of $|F_{\text{TMV-Hg}}|-|F_{\text{TMV}}|$ in this region are compared with $2J_u(2\pi Rr_{\text{Hg}})$ for $r_{\text{Hg}} = 56{\cdot}2$ Å, and $u = 46$, 49 and 52. The amplitude of the $2J_u(2\pi Rr_{\text{Hg}})$ curves is derived from the experimentally determined scale of the $J_0$ contribution of mercury (Fig. 7). There is good agreement between the experimental amplitude difference curve and $2J_{49}(2\pi R \times 56{\cdot}2)$ in the region where the $J_u$ term for TMV is small (Fig. 8(*c*)). The two dips in the experimental difference curve correspond with maxima

* It is, of course, theoretically possible that the relative phases of the $J_u$ terms for TMV and for Hg at the position of the first peak of the Hg term might be such that the resultant intensity is equal to that of the TMV term alone. However, this possibility can be eliminated because, at values of $R$ less than 0·13 Å$^{-1}$, there is, in TMV, no $J_u$ term strong enough to combine in this way with the Hg term.

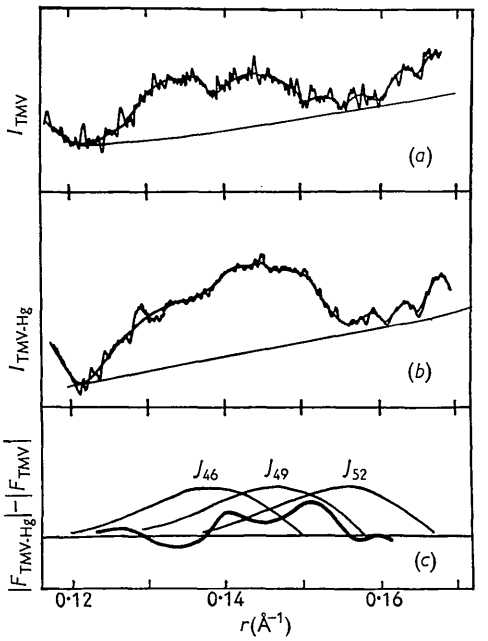


Fig. 8. Determination of the helical parameter, $u$.

($a$) Photometer trace of $I_{TMV}$ on the equator for values of $R$ from 0·12 to 0·17 Å$^{-1}$. The smooth curve shows the values read.

($b$) Photometer trace of $I_{TMV\text{-}Hg}$ on the equator for values of $R$ from 0·12 to 0·17 Å$^{-1}$. The intensity scale is here 1·4 times greater than that of ($a$).

($c$) The difference between $|F_{TMV\text{-}Hg}|$ and $|F_{TMV}|$ (heavy curve), is compared with the first peak of the functions $J_{46}(2\pi R \times 56{\cdot}2)$, $J_{49}(2\pi R \times 56{\cdot}2)$ and $J_{52}(2\pi R \times 56{\cdot}2)$. It is clear that the largest values of $|F_{TMV\text{-}Hg}|-|F_{TMV}|$ occur in the region of the first peak of $J_{49}(2\pi R \times 56{\cdot}2)$, indicating that there are 49 units of TMV protein in the axial repeat period of 69 Å (see text).

in the TMV curve (Fig. 8($a$)) and so indicate that the Hg and TMV contributions to the $J_u$ term are in nearly opposite phase.

The measurements thus establish that the value of $u$ for the mercury helix is 49. It follows, for reasons given above, that there are 49 structure units of TMV protein in the axial repeat period of 69 Å (i.e. one structure unit for each helical net point).

We have seen that there may be either 1 or 2 chemical sub-units (and hence either 1 or 2 Hg sites) per helical net point according to whether the helical structure has symmetry $s$ or $s2$. We are now in a position to decide between these two possibilities.

Since there are 49 helical net points in a 69 Å length of the virus particle, there is one net point for each 1·4 Å length of the particle. Recent estimates of the molecular weight and length of the TMV particle range from 40 to $50 \times 10^6$ and from 3,000 to 3,700 Å respectively (Williams & Steere, 1951; also, Schramm & Bergold, 1947; Oster, Doty & Zimm, 1947; Oster, 1950; O'Konski & Haltner, 1956; Rowen & Ginoza, 1956; Wippler, 1956). On the basis of these measurements, the weight of a 1·4 Å length of the particle lies between 16,500 and 23,000. Since the molecular weight of the chemical sub-unit is 17,000–18,000 (Knight, 1954; Schramm & Braunitzer, 1953), it is clear that there is only one chemical sub-unit to each helical net point.

The same conclusion can be reached from a consideration of the density and radius of the virus particle instead of its weight and length. The density of the dry virus is 1·305 g.cm.$^{-3}$ (J. T. Finch, unpublished). The mean radius lies between 70 and 80 Å (Franklin & Klug, 1956). From this it follows that the 'molecular weight' of a 1·4 Å length of the virus particle lies between 17,000 and 22,000, and thus corresponds with the weight of a single chemical sub-unit.

Thus the TMV structure belongs to the simplest helical line-group, $s$, and contains 49 protein sub-units on 3 turns of the helix in the axial repeat period of 69 Å.

### Derivation of the radial density distribution

The radial density distribution in TMV was calculated from the $F$ curve shown in Fig. 6($a$). To reduce cut-off effects, the $F$ values were first multiplied by an 'artificial temperature factor' of $\exp[-11{\cdot}8^2R^2]$, which has the value 0·25 at the cut-off position, $R = 0{\cdot}10$ Å$^{-1}$. Values of $F$, modified in this way, were taken at intervals in $R$ of 0·002 ($= \delta R$) and used to calculate the function

$$\varrho(r) = 2\pi \sum_R RF(R)J_0(2\pi Rr)\delta R \qquad (3)$$

at intervals of 2·0 Å in $r$, for $r = 0$ to $r = 100$ Å. Here $\varrho(r)$ is the difference between the electron density of the virus particle and that of the solution around it.

We did not have facilities for measuring directly the central peak of the $F$ curve, which is confined to values of $R$ less than 0·0076 Å$^{-1}$. Accurate measurement in this region is difficult, not only because of the low angles involved, but also because of the very rapid variation of intensity with angle. We therefore assumed that, in this region, scattering by the TMV particle would be indistinguishable from that of an equivalent uniform-density cylinder, and would thus have the form of the first peak of $J_1(2\pi Rr_0)/2\pi Rr_0$, where $r_0$ is the radius of the equivalent cylinder. (This device was used earlier in calculating the cylindrical Patterson function of TMV (Franklin, 1955) and also by Caspar (1955) in his work on the radial density distribution.) The value of $r_0$ was chosen such that the first zero of $J_1(2\pi Rr_0)/2\pi Rr_0$ coincides with the first zero on the experimental intensity curve.

The summation of equation (3) was carried out separately for experimental $F$ values in the range $R = 0{\cdot}008$–$0{\cdot}10$ Å$^{-1}$ and for the theoretical central peak. The scale of the theoretical part of the transform was then adjusted with respect to that of the experimental part in such a way that the sum of the two

parts, $\varrho(r)$, had no appreciable negative values, and yet fell to zero at the largest values of $r$. The two components of $\varrho(r)$, calculated in this way, are shown in Fig. 9, and their sum is shown in Fig. 10.

A refinement of the theoretically derived component of $\varrho(r)$ was made by using the values of $\varrho(r)$ arrived at as above to *calculate* the values of $F$ for the central diffraction maximum, by means of the summation

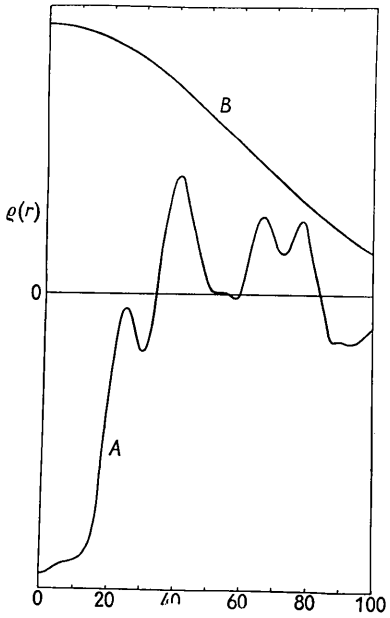


Fig. 9. Curves $A$ and $B$ represent two components of $\varrho(r)$, the difference between the electron density of the virus particle and that of the solution around it. Curve $A$ is the Fourier–Bessel transform of the experimental $F$ values in the range $R = 0{\cdot}008$–$0{\cdot}10$ Å$^{-1}$, and curve $B$ is the transform of the theoretically derived $F$ values of the central peak (see text).

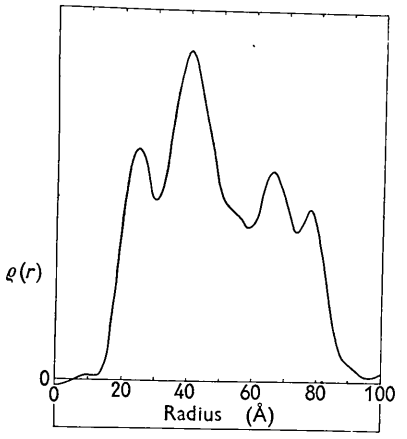


Fig. 10. The radial density distribution of TMV before refinement of the contribution of the central diffraction peak. $\varrho(r)$ is the difference between the electron density of the virus particle and that of the solution around it, and is obtained by adding the ordinates of curves $A$ and $B$, Fig. 9.

$$F(R) = 2\pi \sum_r r\varrho(r) J_0(2\pi Rr)\delta r \,. \qquad (4)$$

The transform of the central peak so derived was then calculated, using equation (3), and added to the experimentally derived component of $\varrho(r)$.

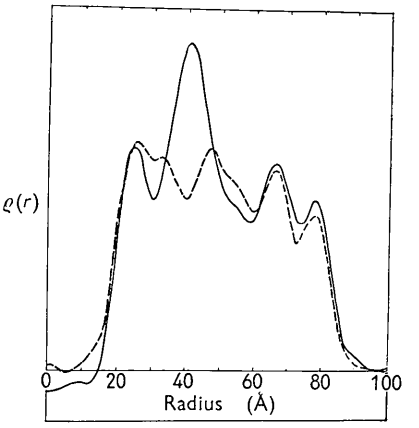


Fig. 11. The full-line curve gives the radial density distribution of TMV after refinement of the contribution of the central diffraction peak, as described in the text. The broken curve gives the radial density distribution of the repolymerized, RNA-free virus protein. The strong density maximum at 40 Å in TMV is replaced by a minimum in the RNA-free protein, indicating that the phosphate–sugar backbone of the RNA molecules lies at this radius.

The $\varrho(r)$ curve derived in this way is shown by the full-line curve in Fig. 11. This differs little from Fig. 10. There is therefore nothing to be gained by making further refinements of the central peak of the $F$ curve.

## Interpretation of the radial density distribution

The interpretation of the radial density distribution in TMV has been discussed elsewhere (Caspar, 1956; Franklin, 1956; Franklin, Klug & Holmes, 1956) and will be considered only briefly here. Clearly the virus particle has a hollow core of radius about 20 Å, and a maximum radius of 80–90 Å. A series of well defined density maxima at values of $r$ ranging from 24 Å to 80 Å must be related to the molecular structure of the protein and nucleic acid components of the virus.

Schramm (1947) and others have shown how it is possible to obtain RNA-free TMV protein in a form in which it bears a strong structural resemblance to the protein of the intact virus. (This is achieved by depolymerizing the virus protein with dilute alkali, extracting the RNA by electrophoresis, and then repolymerizing the protein by lowering the pH.) The radial density distribution of this repolymerized, RNA-free virus protein, determined by the methods described above, has been reported previously (Franklin, 1956), and is shown by the broken curve in Fig. 11. The two curves of Fig. 11 are very similar except in the region of $r = 40$ Å, where the strong density peak

in the TMV curve is replaced by a sharp minimum in the density of the RNA-free protein. We therefore conclude that the phosphate–sugar backbone chain of the RNA lies at a distance of about 40 Å from the particle axis.

The sharpness of the other density maxima, which must be due to the virus protein, suggests that the principal chain directions of the protein molecules lie in a series of coaxial cylindrical surfaces. This is consistent with an earlier suggestion, based on the cylindrical Patterson function of TMV (Franklin, 1955), that the protein chain directions are approximately perpendicular to the particle axis, and tangential rather than radial.

For more detailed information concerning the molecular arrangement of the protein and RNA components of the virus, a quantitative study of the non-zero layer lines of the TMV fibre diagram is required.

### The relative magnitude of $F_{Hg}$ in TMV-Hg

The procedure described above for the determination of the scale of the low-angle, experimentally inaccessible part of the TMV scattering curve leads to the determination of the value of $F_{TMV}$ at $R = 0$. Extrapolation of the term $AJ_0(2\pi Rr_{Hg})$, shown in Fig. 7, gives the value of $F_{Hg}$ at $R = 0$. Comparing the two values, we find that, at $R = 0$, $F_{Hg}$ is approximately 5% of $F_{TMV}$. Theoretically, for one Hg atom per 20,000 molecular weight of virus, and a partial specific volume of 0·73 cm.$^3$g.$^{-1}$ (Bawden & Pirie, 1937; Lauffer, 1944) for the virus, $F_{Hg}$ should be rather less than 3% of $F_{TMV}$.

We have no very satisfactory explanation of this discrepancy. However, a similar unexpectedly high contribution of the mercury is found on the 3rd layer line of TMV-Hg, and we believe the effect to be outside the range of experimental error. There seem to be only two types of explanation possible: either the structure factor of the TMV is less than the expected value, or that of the mercury is greater (our data are not on an absolute scale). The first alternative could arise if the TMV carries with it, throughout the process of purification, an ion atmosphere such that, when the solution is highly concentrated, the particles are, effectively, suspended in a medium of electron density greater than that of water. This would result in a decrease in the effective scattering power of the protein and RNA, especially at low angles. The other possibility is that the bound mercury attracts ions from the solution to its immediate neighbourhood, so that the effective 'heavy atom' is more than the mercury alone.

This work was supported by the Agricultural Research Council.

### References


Bawden, F. C. & Pirie, N. W. (1937). *Proc. Roy. Soc.* B, **123**, 274.

Bernal, J. D. & Fankuchen, I. (1941). *J. Gen. Physiol.* **25**, 111.

Bragg, W. L. & Perutz, M. F. (1952). *Proc. Roy. Soc.* A, **213**, 425.

Braunitzer, G. (1954). *Z. Naturforsch.* **96**, 675.

Bunn, C. W. & Howells, E. R. (1954). *Nature, Lond.* **174**, 549.

Caspar, D. L. D. (1955). Thesis, Yale University.

Caspar, D. L. D. (1956). *Nature, Lond.* **177**, 928.

Crick, F. H. C. (1954). *Science Progr.* **166**, 205.

Franklin, R. E. (1955). *Nature, Lond.* **175**, 379.

Franklin, R. E. (1956). *Nature, Lond.* **177**, 929.

Franklin, R. E. & Gosling, R. G. (1953). *Nature, Lond.* **171**, 740.

Franklin, R. E. & Klug, A. (1956). *Biochim. Biophys. Acta*, **19**, 403.

Franklin, R. E., Klug, A. & Holmes, K. C. (1956). *CIBA Foundation Symposium on Nature of Viruses*, p. 39. London: Churchill.

Green, D. W., Ingram, V. M. & Perutz, M. F. (1954). *Proc. Roy. Soc.* A, **225**, 287.

Harris, J. I. & Knight, C. A. (1952). *Nature, Lond.* **170**, 613.

Harris, J. I. & Knight, C. A. (1955). *J. Biol. Chem.* **214**, 215.

Klug, A., Crick, F. H. C. & Wyckoff, H. W. (1958). *Acta Cryst.* **11**, 199.

Knight, C. A. (1954). *Advances in Virus Research*, **2**, 153.

Lauffer, M. A. (1944). *J. Amer. Chem. Soc.* **66**, 1188.

Niu, C. I. & Fraenkel-Conrat, H. (1955*a*). *Biochim. Biophys. Acta*, **16**, 597.

Niu, C. I. & Fraenkel-Conrat, H. (1955*b*). *J. Amer. Chem. Soc.* **77**, 5882.

O'Konski, C. T. & Haltner, J. (1956). *J. Amer. Chem. Soc.* **78**, 3604.

Oster, G. (1950). *J. gen. Physiol.* **33**, 445.

Oster, G., Doty, P. M. & Zimm, B. H. (1947). *J. Amer. Chem. Soc.* **69**, 1193.

Rowen, J. W. & Ginoza, W. (1956). *Biochim. Biophys. Acta*, **21**, 416.

Schramm, G. (1947). *Z. Naturforsch.* **2b**, 112, 249.

Schramm, G. & Bergold, G. (1947). *Z. Naturforsch.* **2b**, 108.

Schramm, G. & Braunitzer, G. (1953). *Z. Naturforsch.* **8b**, 61.

Schramm, G., Braunitzer, G. & Schneider, J. W. (1954). *Z. Naturforsch.* **9b**, 298.

Walker, P. M. B. (1955). *Expt. Cell Research*, **8**, 567.

Watson, J. D. (1954). *Biochim. Biophys. Acta*, **13**, 10.

Wilkins, M. H. F., Stokes, A. R. & Wilson, H. R. (1953). *Nature, Lond.* **171**, 738.

Williams, R. C. & Steere, R. L. (1951). *J. Amer. Chem. Soc.* **73**, 2057.

Wippler, C. (1956). *J. Chim. Phys.* **53**, 329.